JOURNAL OF MATERIALS SCIENCE 25 (1990) 3566-3572

Densification and microstructure development in the reaction sintering process of yttrium iron garnet

R. J. YOUNG, T. B. WU
Department of Materials Science and Engineering, National Tsing Hau University, Hsinchu, Taiwan

I. N. LIN
Chung-Shan Institute of Science and Technology, Lung-Tan, Taiwan

Factors affecting the densification and microstructure development in the reaction sintering process (RSP) of yttrium iron garnet were investigated. Three different powder mixtures were used: Fe_2O_3/Y_2O_3, $Fe_2O_3/YFeO_3$ (1100° C calcined), and $Fe_2O_3/YFeO_3$ (1200° C calcined). The conventionally prepared garnet powder was also adopted as a reference material. It was found that the RSP using Fe_2O_3–$YFeO_3$ systems has a beneficial effect on densification from the dilatation occurring along with the reaction of garnet formation. On the other hand, it has a detrimental effect due to the local contraction induced by the reaction in the Fe_2O_3–Y_2O_3 system. The densification rate and ultimate density achievable are also affected by the $YFeO_3$ powder adopted in RSP. A high grain-growth rate was obtained for garnet when the 1200° C calcined $YFeO_3$ powder was used. This leads to a high densification rate at low temperature. However, the densification ability deteriorates at temperatures above 1425° C due to the trap of pores in the fast-grown grains. Conversely, the grain-growth rate in RSP with 1100° C-calcined $YFeO_3$ was moderate, and although it gives a slower densification rate at low temperature, the ultimate density can be raised to $\approx$99% theoretical density at $\geqslant$1450° C.

1. Introduction

The yttrium iron garnet (YIG) ceramics of the formula $Y_3Fe_5O_{12}$ have been studied extensively due to their superior magnetic properties at microwave frequency [1]. High density and uniform microstructure of controlled grain size are desirable in this material to minimize the energy loss at this high frequency. It is difficult to reach a high density close to theoretical value through the conventional ceramic process, i.e. via mixing, calcining, pressing and sintering of powders made of mixed oxides of Y_2O_3 and Fe_2O_3. This is due to the refractory nature and high hardness of the garnet materials. Some unconventional processes for preparing ceramic materials have been developed to circumvent this difficulty, including the hot-pressing technique [2–4] and sintering of ultra-fine powders which are prepared by the chemical coprecipitation method [5–8].

The reaction sintering process (RSP), in which a chemical reaction between the constituents is involved during sintering, has been applied successfully in processing of mullite [9], TiB_2 [10], SiC [11], Si_3N_4 [12] and TiC [13]. The mechanism by which the RSP technique is beneficial for densifying the materials difficult to sinter is the high driving force arising from the chemical reaction involved. It is two or three orders of magnitude greater than the driving force caused by the surface energy of solid-state diffusion [14]. This technique has also been applied successfully for preparing high-density YIG materials, using the Fe_2O_3 and $YFeO_3$ as the major constituents [15].

There are, however, problems such as reaction kinetics, densification behaviour and formation mechanism for the remaining microstructure development. Understanding of all the factors is important to ensure the successful application of the RSP technique. In this study, special reacting systems are designed to study the detailed mechanism involved in densification and microstructure development of the YIG materials.

2. Experimental procedure

Chemically pure Fe_2O_3 (99.9% purity) and Y_2O_3 (99.99% purity) powders were used as starting materials. The conventional ceramic process is followed for preparing the garnet powders, which is used as a reference for studying the densification kinetics. The powder mixture of the formula $Y_3Fe_5O_{12}$ (Y_2O_3 : Fe_2O_3 = 3 : 5) is blended in ethanol for 24 h using plastic bottles and Teflon balls, calcined at 1300° C for 3 h in air and then pulverized in ethanol with tungsten carbide balls for 3 h. This material is referred to as G_3 material.

The orthoferrite powders are prepared by a similar procedure as that for preparing G_3 powders. The powder mixtures with a formula $YFeO_3$ (Y_2O_3 : Fe_2O_3 =

0022–2461/90 $03.00 + .12

1 : 1) are calcined either at 1100° C or 1200° C for 3 h. The orthoferrite powders thus obtained are then mixed with Fe_2O_3, at the ratio $Fe_2O_3 : YFeO_3 = 1 : 3$, and are referred as P_1 and P_2 materials, respectively. Another mixture which contained Y_2O_3 and Fe_2O_3, ratio 3 : 5, is also prepared and is referred as M_0 material.

The four categories of powder, i.e. G_3, P_2, P_1 and M_0, were then pelleted and sintered. The sintering was proceeded at a temperature range from 1350 to 1475° C for 1, 2, 4, 8 and 16 h, respectively. The density of the sintered pellets was measured by a buoyancy technique. The linear shrinkage of the samples, 5.0 (ϕ) × 2.0 (t) mm, was examined from room temperature to 1450° C under a heating rate of 5° C min^{-1} by thermal dilatometry. The evolution of microstructure was investigated by examining the as-sintered surface of green-compact, 1300° C, 0 h, 1400° C, 1 h and 1400° C, 16 h sintered samples, with a scanning electron microscope (SEM).

3. Results

3.1. Densification behaviour

The densification behaviour for samples sintered at 1400° C are shown in Fig. 1. The density of P_2 samples already reaches 94.0% theoretical density (TD) for only 1 h of sintering at 1400° C. It increases moderately with soaking time thereafter to 97.8% TD after 8 h of sintering, and then slightly drops to 97.3% TD at 16 h of sintering. The other three samples (P_1, M_0 and G_3) densify at a slower rate. The density of P_1 samples increases from 81% TD with soaking time and reaches 94.3% TD after 16 h of sintering. The densification of G_3 and M_0 samples are even inferior to that of P_1.

The temperature dependence of densification of the four samples after 1 h of sintering are shown in Fig. 2. The P_2 samples still show the best densification for sintering at temperatures below 1450° C. A high density of 98.2% TD is reached at 1425° C. However, it then slightly drops to 97.9% TD at 1475° C. On the other hand, the densification of P_1 samples progressively increases with rising temperature and reaches 98.2% TD at 1475° C. The G_3 samples possess a lower densification than P_1 and P_2 at low temperatures ($\leqslant$ 1400° C) and then a high densification of 96% TD is rapidly reached for sintering at 1425° C. However, it is nearly unchanged for sintering at higher temperatures, i.e. 1450 and 1475° C. The M_0 samples show the worst densification of all: the highest density it reaches is only 94.0% TD at 1475° C.

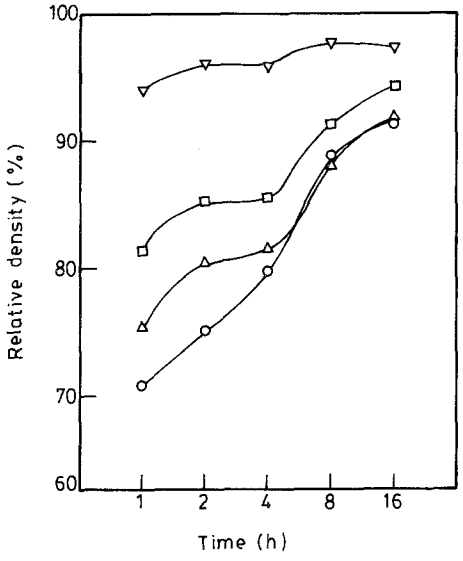

Figure 1 Densification–time characterisitics of G_3, M_0, P_1 and P_2 samples, sintered at 1400° C. △, G_3; ○, M_0; □, P_1; ▽, P_2.

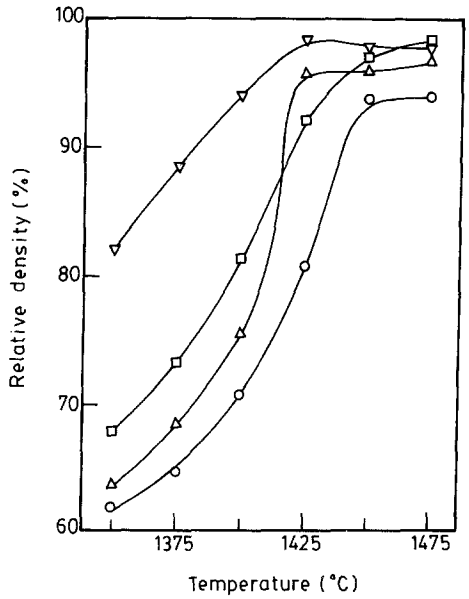

Figure 2 Densification–temperature characterisitics of G_3, M_0, P_1 and P_2 samples, sintered for 1 h. Symbols as Fig. 1.

The ultimate density reachable for the four sample categories and their correlative sintering conditions are listed in Table I. It can be seen that the P_1 and P_2 samples possess superior densification ability, while the M_0 samples have inferior densification ability as compared to that of G_3 samples. Also, although P_1 and P_2 samples have similar constituents (Fe_2O_3 and $YFeO_3$) their densification behaviours are not quite the same. The P_1 samples have a lower densification rate at low temperature, but the rise in sintering temperature can effectively improve the densification to a high density close to the theoretical value, $\approx$ 99% TD. Conversely, the P_2 samples show better densification at low temperature, but become deteriorated at temperatures above 1425° C.

The dynamic densification behaviour of the four samples, measured from dilatometry, are shown in Fig. 3. It is revealed that in the conventional sintering process, the sample (G_3) progressively shrinks at temperatures above 900° C. However, in the reaction sintering process (RSP), the M_0, P_1 and P_2 samples

TABLE I Ultimate density and correlative sintering conditions of G_3, M_0, P_1 and P_2 samples

	G_3	M_0	P_1	P_2
Ultimate density (% TD)	96.7	96.0	98.8	98.3
Sintering conditions (Temp/time)	1475° C/1 h	1425° C/8 h	1450° C/8 h	1425° C/8 h

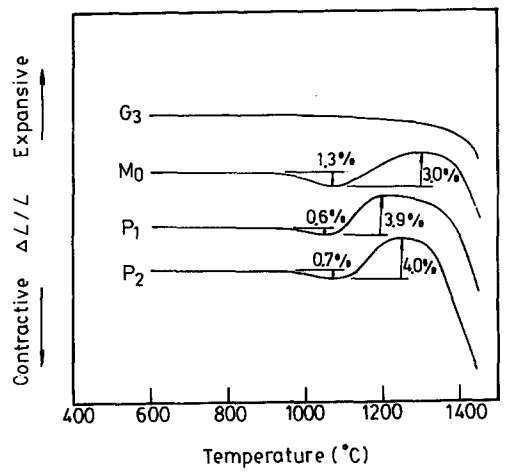

Figure 3 Dilatometry of G_3, M_0, P_1 and P_2 samples.

experience dilatation at temperature around 1050 to 1300° C, followed by major shrinkage above 1300° C. It is also noticed that for the M_0 sample, a significant volume shrinkage has appeared prior to dilatation; however, for the other two samples, P_1 and P_2, the volume shrinks only slightly before the dilatation takes place.

2.2. Microstructure development

The evolution of microstructure in the four groups of samples are shown in Figs 4 to 7, where the surface morphologies of as-sintered samples corresponding to four stages of sintering are demonstrated. The granular structure of the green, initial, intermediate and final stages of sintering are represented by the microstructures of (a) green compact; (b) samples sintered at 1300° C without soaking; (c) samples sintered at 1400° C for 1 h; and (d) samples sintered at 1400° C for 16 h, respectively.

For the G_3 materials, the green pellet consists of garnet powders of bimodal structure, i.e. the fine (1 μm) particles are distributed among the coarse (5 μm) particles (Fig. 4a). Both the fine and coarse particles coalescence into grains at initial stage of sintering, and the bimodal structure is still observed, as shown in Fig. 4b. A non-uniform granular structure of 2 to 5 μm, which is evidently the growth of the two sizes of grains, is developed at an intermediate stage of sintering as shown in Fig. 4c. A number of pores still remain, resulting in a relatively low density ($\approx$ 75.4% TD) of the sintered body. The granular structure has become better packed with some pores still observable at the final stage of sintering (Fig. 4d).

For the M_0 materials, the green-compact morphology as shown in Fig. 5a consisted of uniformly mixed ultra-fine Fe_2O_3 powders ($\approx$ 0.2 μm) and Y_2O_3 particles of 2 μm size. At the initial stage of sintering, the fine powders of sub-micrometre size are sintered together with the large particles (Fig. 5b). It is interesting to note that the large grains ($\sim$ 4 μm) are actually agglomerates of tiny grains of sub-micrometre size. This is attributed to the reaction that takes place during sintering in the Fe_2O_3–Y_2O_3 system. This phenomenon affects significantly the sintering behaviour of a later stage, which will be discussed in detail

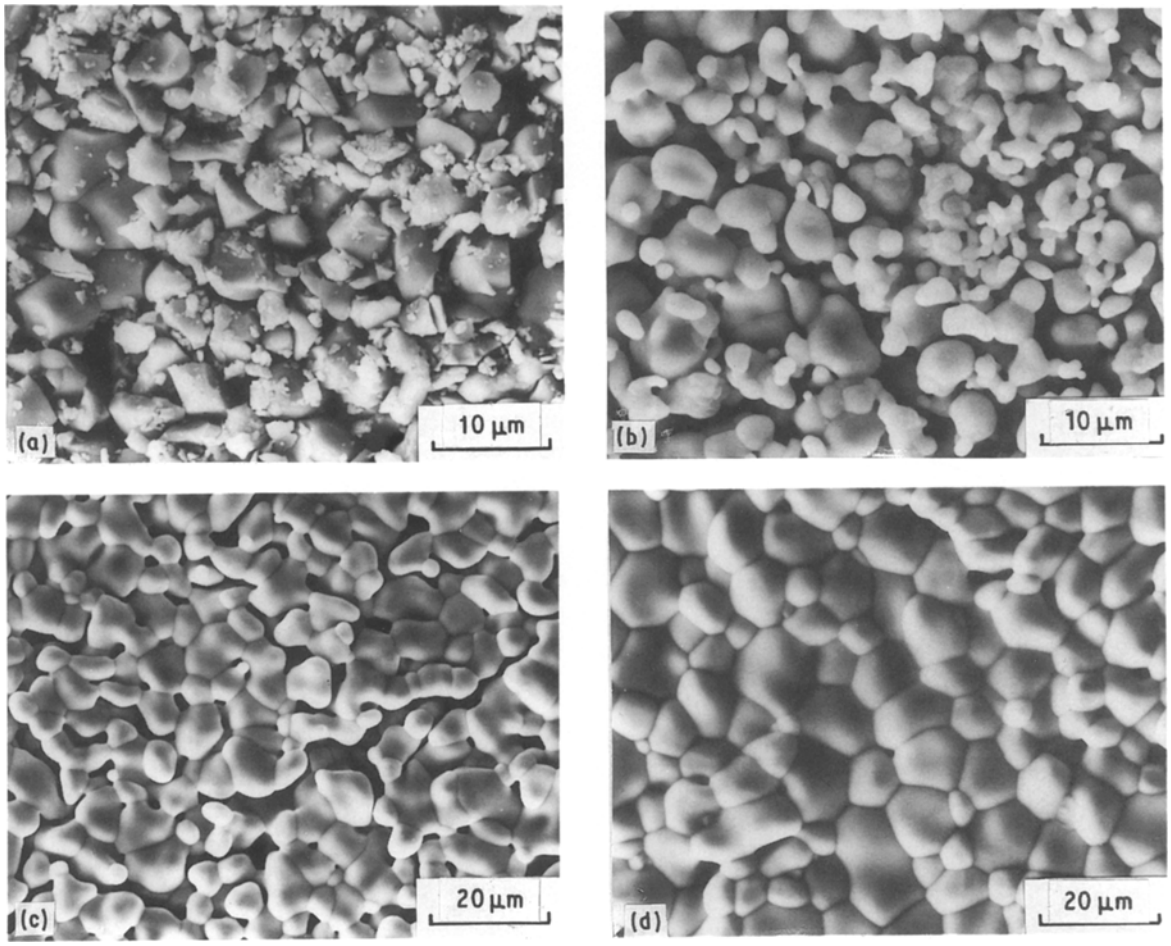

Figure 4 Surface morphologies of G_3 sample at conditions of (a) green compact; (b) heating to 1300° C without soaking; (c) sintering at 1400° C for 1 h; (d) sintering at 1400° C for 16 h, as observed by scanning electron microscopy.

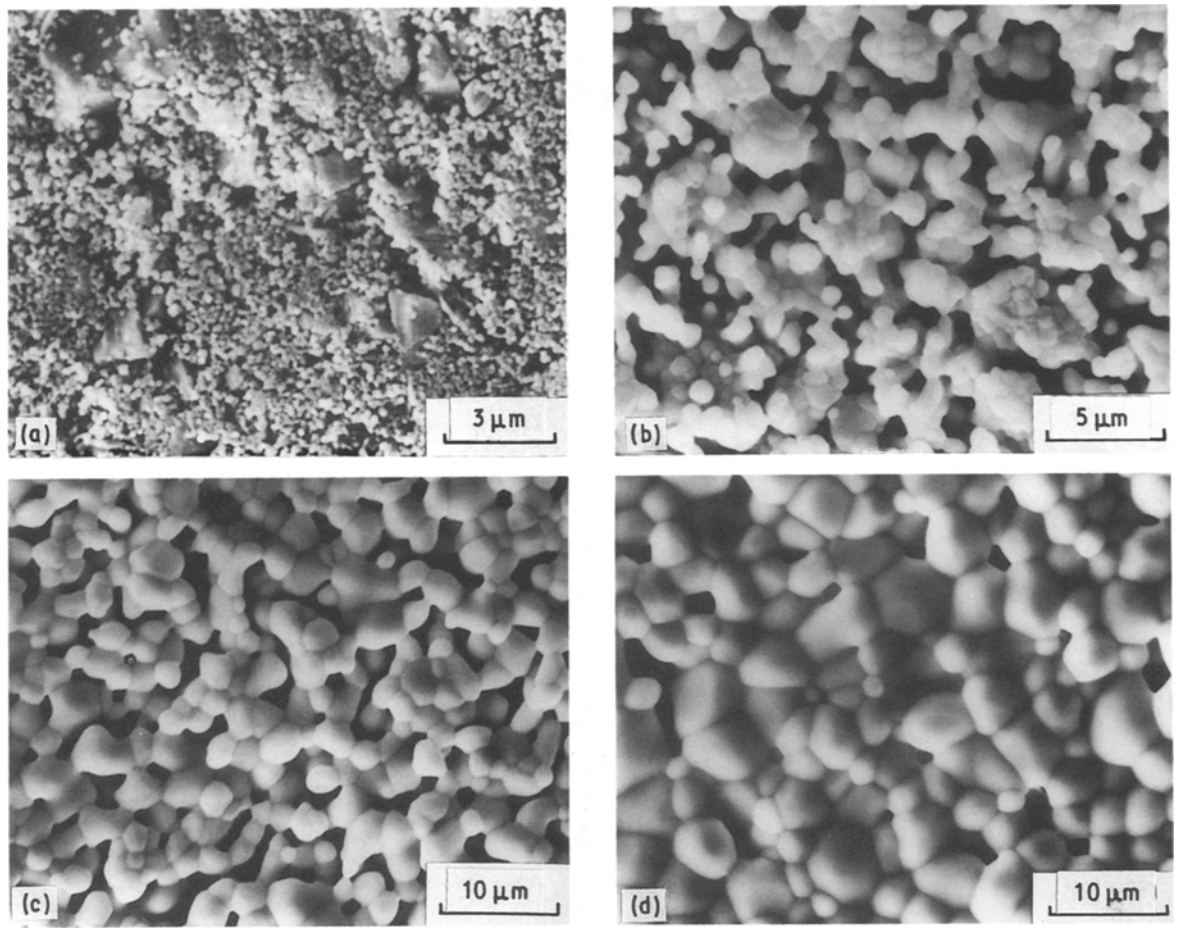

Figure 5 Surface morphologies of M_0 sample at conditions of (a) green compact; (b) heating to 1300° C without soaking; (c) sintering at 1400° C for 1 h; (d) sintering at 1400° C for 16 h, as observed by scanning electron microscopy.

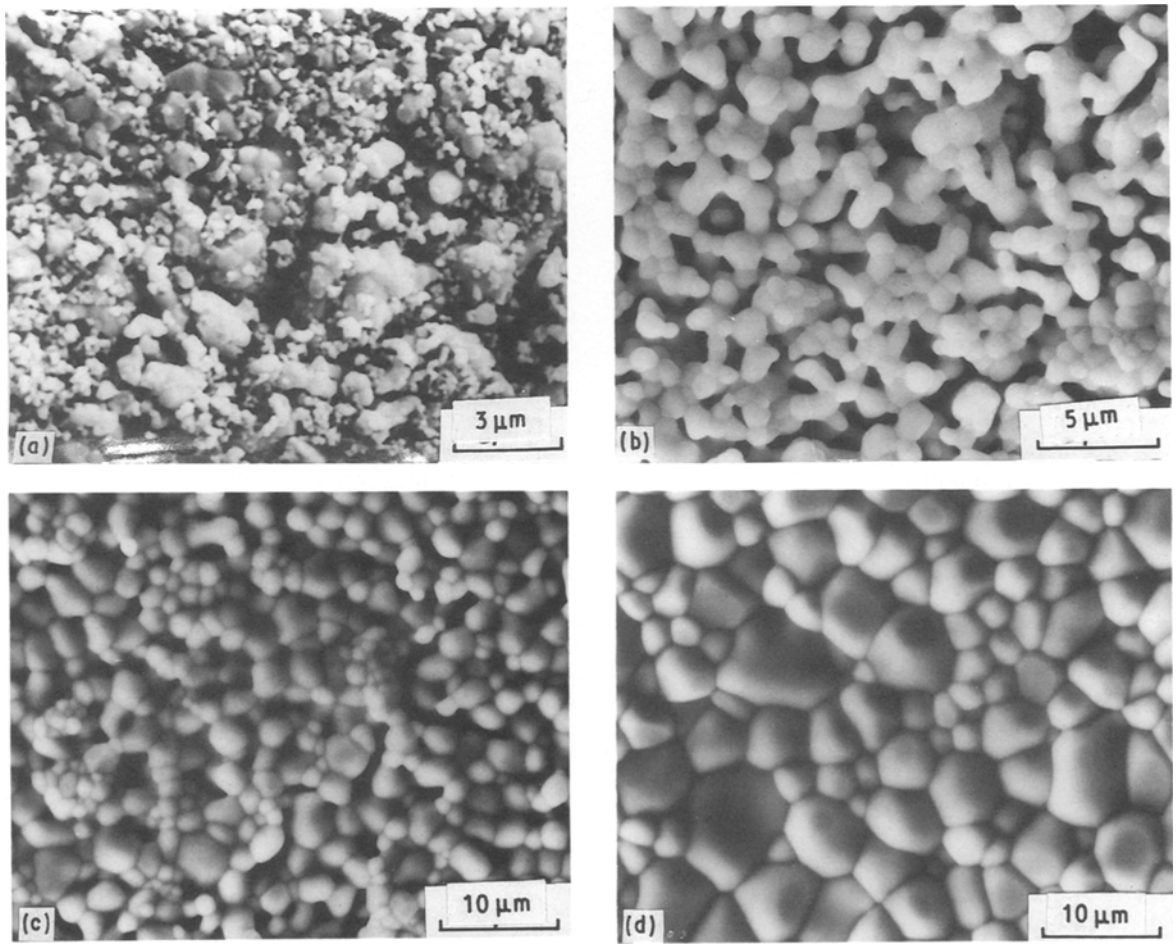

Figure 6 Surface morphologies of P_1 sample at conditions of (a) green compact; (b) heating to 1300° C without soaking; (c) sintering at 1400° C for 1 h; (d) sintering at 1400° C for 16 h, as observed by scanning electron microscopy.

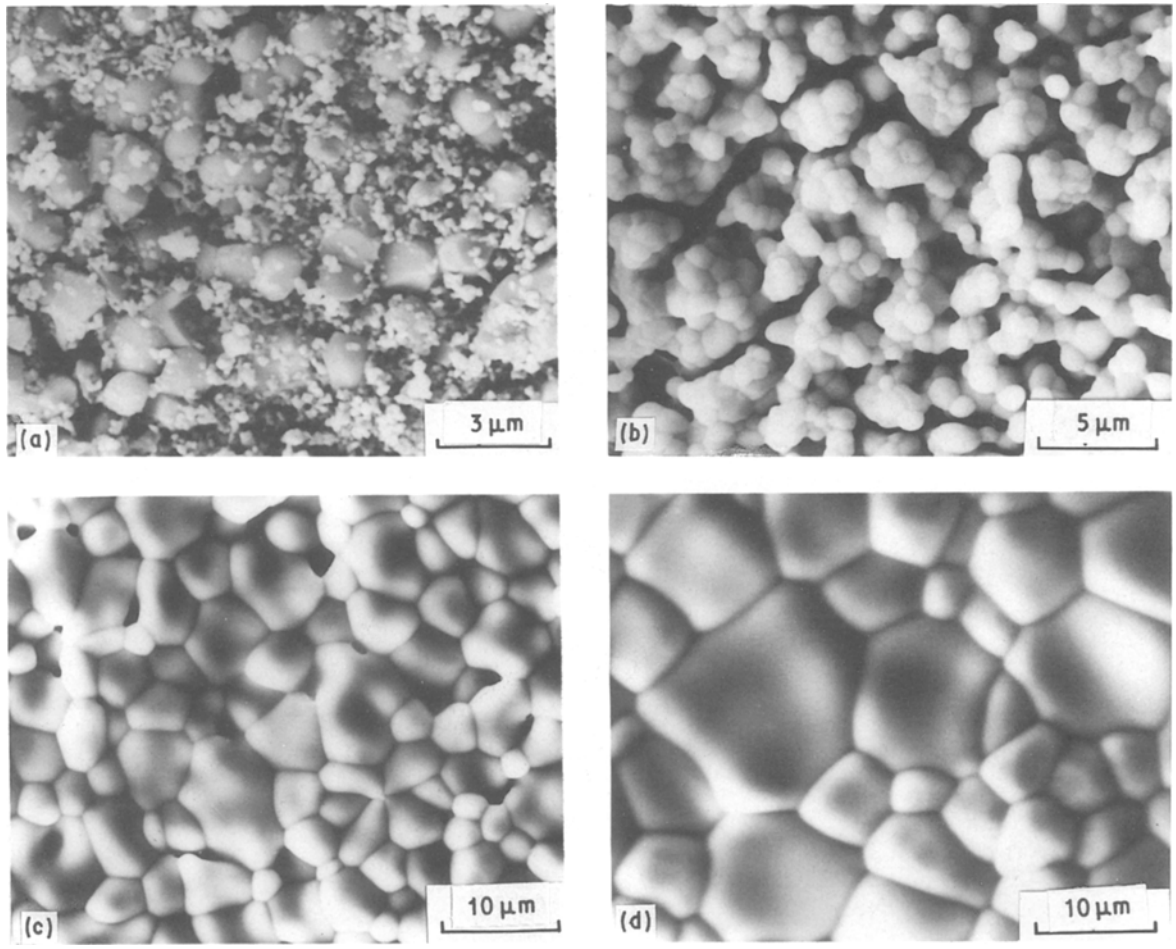

Figure 7 Surface morphologies of P_2 sample at conditions of (a) green compact; (b) heating to 1300° C without soaking; (c) sintering at 1400° C for 1 h; (d) sintering at 1400° C for 16 h, as observed by scanning electron microscopy.

below. The grains then grow to a highly porous granular structure, as in Fig. 5c, at the intermediate stage of sintering. An inhomogeneous granular structure results at the final stage of sintering, with quite a few large pores remaining on the surface, as shown in Fig. 5d.

Figs 6a and 7a reveal that the green-compact of P_1 and P_2 materials also consists of a bimodal structure. The sub-micrometre Fe_2O_3 powders are distributed among the large orthoferrite particles. The 1200° C-calcined orthoferrite particles are somewhat larger than the 1100° C-calcined particles. Both are around 1 to 2 μm. At the initial stage of sintering, similar microstructures to that in Fig. 5b, but more uniform and better packed, are observed (Figs 6b and 7b); namely, the fine grains are connected with the large garnet particles and the latter are agglomerates of tiny grains of sub-micrometre size. The sizes of the grains in the agglomerates are the same as those of individual grains. There are more single grains existing in P_1 materials and most of the particles are large agglomerates in the P_2 materials.

The microstructures at the intermediate stage of sintering are shown in Figs 6c and 7c for P_1 and P_2 materials, respectively. The granular structure is coarser and less porous for P_2 material. The sintered density of this material (94% TD) is, therefore, much higher than that of the P_1 material (81% TD). On extending the soaking time at 1400° C to 16 h, closely packed granular structure results for both P_1 and P_2 materials, as shown in Figs 6d and 7d. Clearly, the latter has a better densified microstructure (97.3% TD) than the former (94.3% TD).

4. Discussion

From the previous result for the sintered density of the four groups of samples (M_0, P_1, P_2 and G_3) it is noted that the ultimate density attainable for G_3 and M_0 materials is low, while that for P_1 and P_2 materials is high. This is intimately related to the densification mechanisms. Only solid-state diffusion can occur during the sintering of G_3 materials, since their powders are prepared by the conventional calcination and pulverization procedures. There are two drawbacks to this process. The first is the non-uniformity in particle size distribution of the powder as indicated in Fig. 4a, which arises from the difficulty in pulverizing the extremely high hardness (≈ 8.5) garnet particles. The other is the low sinterability of the large garnet particles, according to Herring's scale law [16]. The anomalous grain growth at high temperature is therefore easily initiated, as shown in our previous work [15]. The inhomogeneous granular structure and low sintered density are thus expected.

The reaction sintering process for preparing YIG materials is thus applied to circumvent the said difficulties. The chemical reaction of Fe_2O_3 with either $YFeO_3$ or Y_2O_3 to initiate the formation of $Y_3Fe_5O_{12}$

garnet is involved. The densification and microstructural development are expected to be enhanced. Sztaniszlav *et al.* [17] have indicated that the orthoferrite ($YFeO_3$) will appear as the intermediate phase in the synthesis of garnet ($Y_3Fe_5O_{12}$) from oxides (Y_2O_3 and Fe_2O_3). In other words, the following reactions occurred sequentially

$$Y_2O_3 + Fe_2O_3 \rightarrow 2YFeO_3 \quad (1)$$

$$YFeO_3 + Fe_2O_3 \rightarrow Y_3Fe_5O_{12} \quad (2)$$

The first reaction takes place in the temperature ranging from 800 to 1100° C, and the second starts at 1100° C and completes at 1300° C. The three reaction sintering processes utilized, however, behave quite differently in densification rate and microstructural evolution. The sintering density is improved drastically for P_1 and P_2 materials, while it is degraded seriously for M_0 materials. The question now raised is, what is the mechanism which causes such large discrepancies in these three RSP routes? The key must be hidden in the reaction sequences mentioned in Equations 1 and 2.

It has been evaluated theoretically from the X-ray density of the four compounds involved in the reaction that about 10.0% of volume contraction will occur for orthoferrite-phase formation in Equation 1 and 7.5% of volume expansion will occur for garnet-phase formation in Equation 2 [15]. The dilatometry result for the M_0 sample, shown in Fig. 3, has indeed revealed the above two consecutive volume changes at temperature regions corresponding to the occurrence of Equations 1 and 2. However, it is noted that the volume change induced from the first reaction does not have a good response in the dilatometry, as compared to that from the second reaction. This indicates that local volume contraction takes place where the orthoferrite being formed has occurred in the M_0 sample after the first reaction. For the sintering of P_1 and P_2 specimens, the volume expansion induced from the garnet formation is also clearly observed from the dilatometry shown in Fig. 3. Although a weak volume contraction has also occurred prior to volume expansion, it undoubtedly comes from the coalescence of particles, because there is no other chemical reaction than the garnet formation between Fe_2O_3 and $YFeO_3$.

Before investigating the kinetics of RSP further, an interesting phenomenon should be examined in detail. At the initial stage of sintering, the large particles in M_0, P_1, and P_2 materials were disintegrated into fine grains, which were later agglomerated. Reasonable as it sounds, the disintegration of particles is, however, quite unbelievable. Another route of microstructure evolution is thus proposed as follows. Walfmerier *et al.* [18] have pointed out that garnet formation from $YFeO_3$ and Fe_2O_3 is controlled by the inward diffusion of iron ions from Fe_2O_3 into $YFeO_3$. If this mechanism is true, there will be tiny grains formed at the surface of orthoferrite, since the particle size of Fe_2O_3 ($\approx 0.2\,\mu m$) is much finer than that of orthoferrite. An agglomerate of garnet grains will be formed replacing the original orthoferrite particle after the completion of the garnet formation reaction, as shown schematically in Fig. 8.

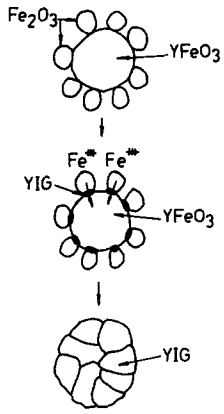

Figure 8 Scheme of garnet formation from the mixture of Fe_2O_3 and $YFeO_3$.

The reaction between fine Fe_2O_3 and coarse Y_2O_3 particles in M_0 material is presumably similar to the Fe_2O_3–$YFeO_3$ system. Since local volume contraction during the reaction occurred in the Fe_2O_3–Y_2O_3 system, the separation of particles might result, as depicted in Fig. 9. On the other hand, the orthoferrite particles might squeeze each other due to the volume dilatation during the reaction in the FE_2O_3–$YFeO_3$ system, as depicted in Fig. 10. The voids which exist in the green compact are thereafter expanded in M_0 materials and are compressed in P_1 and P_2 materials at the initial state of sintering, as observed in Figs 5b, 6b and 7b. Further sintering is thus expected to be retarded for the former (M_0) and promoted for the latter (P_1 and P_2).

The keen effect of calcination temperature on the sintering behaviour of P_1 and P_2 materials is not as obvious as in the previously discussed model. It could be the result of larger orthoferrite particles in P_2 materials as compared to those of P_1 materials. As suggested previously, agglomerates of tiny garnet grains are formed at the sites of orthoferrite particles after the completion of garnet formation. Therefore more large agglomerates will be created in the P_2 sample than in P_1 sample at the initial state of sintering (Figs 6b and 7b). At the intermediate stage of sintering, the tiny grains in each agglomerate are expected to coalesce into single grains. A granular structure with wide grain-size distribution can then be developed in the P_2 sample, and the Ostwald ripening

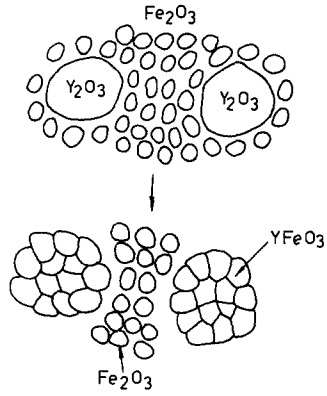

Figure 9 Schematic drawing of particle separation due to local volume contraction induced by orthoferrite formation from Y_2O_3 and Fe_2O_3.

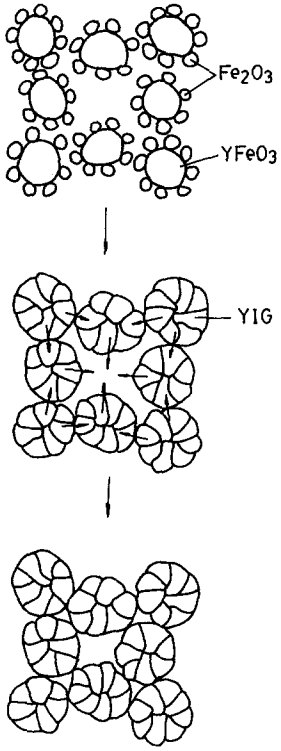

Figure 10 Schematic drawing of particle squeeze due to volume dilatation induced by garnet formation from Fe_2O_3 and $YFeO_3$.

between adjacent grains is thus enhanced. As a consequence, a higher densification rate is achieved for the P_2 sample. However, for sintering at temperatures above 1425° C, the growth rate of grains in the P_2 sample may become too high, and densification ability will be deteriorated due to the trapping of pores in the fast-grown grains. Such a result is indeed observed from optical microscopy of the polished and thermally-etched P_2 sample after sintering at 1450° C for 4 h, as shown in Fig. 11. On the other hand, the P_1 sample has a moderate grain-growth rate at high temperature, and the pores at the grain boundary can be progressively eliminated to reach a high densification close to the theoretical density. Finally, a uniform granular structure of low porosity can be developed, as shown in our previous paper [15].

5. Conclusions

1. The densificaton of yttrium iron garnet (YIG) is enhanced using the reaction-sintering process (RSP), as compared to the conventional calcination and pulverization routes for preparing YIG samples.

2. Materials of sintering density as high as 99% TD can be obtained when prepared from powders of the Fe_2O_3–$YFeO_3$ (calcined at 1100° C) system and sintered at 1450° C for 8 h.

3. The use of 1200° C-calcined $YFeO_3$ in RSP induces a high grain-growth rate and is helpful for densification at low temperatures. However, the densification at temperatures above 1425° C deteriorates due to the trap of pores in the fast-grown grains.

4. RSP using the Fe_2O_3–Y_2O_3 system as starting material will have a deleterious influence on the sintering behaviour of the materials.

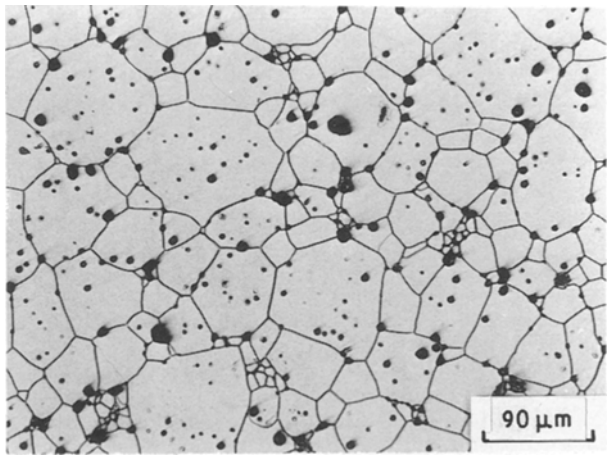

Figure 11 Optical microscopy of polished and thermally-etched P_2 sample sintered at 1450° C for 4 h.

5. The formation of fine-grain YIG aggregates at the initial stage of sintering is thought to be caused by the inward diffusion of iron-ions from the surrounding tiny Fe_2O_3 powders into the coarse $YFeO_3$ or Y_2O_3 particles.

6. RSP will have a beneficial effect on sintering behaviour only when dilatation occurs along with the reaction. It will impose a detrimental effect on densification behaviour if local contraction occurs with the reaction.

References

1. G. R. HARRISON and L. R. HODGES Jr., in "Physics of Electronic Ceramics", edited by L. L. Hench and D.B. Dove (Marcel Dekker, New York, 1972) p. 857.
2. G. R. BLAIR, A. C. D. CHAKLADER and N. M. P. LOW, *Mater. Res. Bull.* **8** (1973) 161.
3. O. PROKASH and C. M. SRIVASTAVA, *ibid.* **15** (1980) 665.
4. G. A. NAZIRIPOUR, *et al.*, *J. Mater. Sci.* **20** (1985) 375.
5. W. P. WOLF and G. P. RODRIGUE, *J. Appl. Phys.* **29** (1958) 105.
6. J. Y. LAVAL, *J. Mater. Sci.* **13** (1978) 1937.
7. M. MULTANI *et al.*, *Mater. Res. Bull.* **14** (1979) 1251.
8. M. S. MULTANI *et al.*, *ibid.* **16** (1981) 1535.
9. P. D. D. RODRIGO and P. BOCH, *Int. J. High Tech. Ceram.* **1** (1985) 3.
10. Y. MIYAMOTO and M. KOIZUMI, *Commun. Amer. Ceram. Soc.* **67** (1984) C–224.
11. O. YAMADA, Y. MIYAMOTO and M. KOIZUMI, *Amer. Ceram. Soc. Bull.* **64** (1985) 319.
12. G. R. TERWILLIGER and F. F. LANGE, *J. Mater. Sci.* **10** (1975) 1169.
13. C. J. QUINN and D. L. KOHLSTEDT, *J. Mater. Sci.* **19** (1984) 1229.
14. R. L. COBLE, in "Sintering-Theory and Practice" edited by D. Kolar, S. Pejovnik and M. M. Ristic (Elsevier Scientific, Amsterdam, 1982) p. 145.
15. R. J. YOUNG, T. B. WU and I. N. LIN, *Mater. Res. Bull.* **22** (1987) 1475.
16. C. HERRING, *J. Appl. Phys.* **21** (1950) 301.
17. A. SZTANISZLAV *et al.*, *J. Mag. Mag. Mater.* **41** (1984) 75.
18. U. WOLFMERIER and W. GUNSSER, in "Reactivity of Solids" Vol. 2, edited by K. Dyrek, J. Habar and J. Nowotny (Polish Scientific Publishers, Warszawa, 1982) p. 1026.

Received 14 March
and accepted 30 August 1989